Experimental Investigation of Liquid Slugging in Reciprocating Compressors

Teo B BALCONI[1], Tadeu T RODRIGUES[2], Cesar J DESCHAMPS[1]*

[1]POLO Research Laboratories for Emerging Technologies in Cooling and Thermophysics
Department of Mechanical Engineering, Federal University of Santa Catarina
88040900 Florianopolis, SC, Brazil

[2]NIDEC-GA, R&D,
Joinville, SC, Brazil

* Corresponding Author: deschamps@polo.ufsc.br

ABSTRACT

Liquid slugging is a phenomenon in which liquid refrigerant enters the compression chamber, posing a significant risk to reciprocating compressors by potentially damaging valves and other components, often leading to failure. Reciprocating compressors adopt suction mufflers to attenuate noise resulting from pressure pulsation brought about by piston. However, the impact of the suction muffler design on liquid refrigerant volume during slugging remains unclear due to intricate fluid dynamics. This paper reports an experimental investigation of the two-phase flow of refrigerant in a simplified suction muffler geometry. The aim is to explore how operating conditions influence the volume of liquid refrigerant reaching the compression chamber after a liquid slugging event. A test bench, comprising a calorimeter, liquid injection system, and test section, was developed was designed to measure the volume of R-134a in its liquid phase at the muffler outlet following a predefined mass injection. The calorimeter was used to submit the muffler to different operating conditions. The injection system included a reservoir of refrigerant in liquid form under controlled pressure, supply line, and a solenoid valve for controlled test section injections. The test section, featuring a sight glass and a transparent acrylic muffler, was integrated into the calorimeter circuit to replicate hermetic compressor operating conditions. A high-speed camera facilitated the observation of flow through the muffler. Results indicate that liquid slugging is highly complex, with the volume of liquid refrigerant reaching the muffler outlet increasing with the injection pressure.

1. INTRODUCTION

Refrigeration systems have refrigerant fluid in vapor, liquid, and two-phase forms. Compressors in these systems are intended to compress only vapor in their compression chambers. However, the presence of liquid, whether refrigerant or oil, in the compression chamber can brought about substantial pressure increase, potentially elevating it to ten times the normal discharge pressure (Singh et al., 1986). This excessive pressure can lead to excessive stress on critical components, including the connecting rod-crank mechanism, valve plate, and valves, thereby reducing the compressor's lifespan (Laughman et al., 2006) and increasing the risk of fractures. Stouppe & Lau (1989) found that liquid slugging accounted for 20% of the failures in reciprocating compressors in air conditioning systems, with these compressors being particularly susceptible due to their higher compression ratios (Liu & Soedel, 1995).

Liquid admission can occur during two specific periods: the compressor start-up, often referred to as flooded start, and ongoing compressor operation. The infiltration of liquid refrigerant can be attributed to several factors: **(i)** excessive refrigerant in the system, **(ii)** extended periods of compressor inactivity, **(iii)** operation in extremely cold temperatures, **(iv)** incomplete evaporation of refrigerant due to low thermal loads or fan malfunction, and **(v)** the use of hot gas defrosting, which is commonly used in the industry as describe in Secop (2019) and Embraco - Nidec (2022).

Few investigations reported in the literature consider the entry of liquid into the compressors (Brendel et al., 2023), but no attention was paid to the flow of liquid through the suction system (muffler). This subject has received little attention, with limited information available. It remains unclear whether the liquid entering through the suction system

can reach the compression chamber, a primary concern. Rodrigues (2018) conducted a numerical study of two-phase liquid-gas flow in four suction muffler designs using the Volume of Fluid (VOF) method. The study analyzed the influence of muffler design on the mass flow rate of liquid reaching the compression chamber in reciprocating compressors. The findings indicate that muffler design significantly impacts the flow towards the compression chamber, with different designs showing varied capabilities to drive liquid towards the cylinder. The numerical procedure provided insights into liquid slugging in the compressor's suction system and highlighted the complexities of this phenomenon.

In a recent study, Bianchi et al. (2021) carried out a numerical evaluation to assess the injection of refrigerant liquid and oil into a muffler with a simplified design. The study aimed to explore the relationship between the volumes of injected and collected liquids after passing through the muffler, using R-134a as the refrigerant. An experimental setup was developed to validate the numerical results, specifically focusing on oil injection. Three different speeds were tested, with 16 ml injections of POE ISO 22 oil. The experimental and numerical results were in good agreement, except for the test conducted at the lowest speed. The authors noted that the volume of liquid reaching the muffler exit increased with the velocity of the liquid at the inlet and highlighted the random variability of the experimental data. In another study by Balconi et al. (2022), the injection of POE ISO 22 oil into a muffler was experimentally evaluated under the flow of R-134a refrigerant. The results revealed a direct correlation between the speed of the oil at the inlet and the volume of oil exiting the muffler and entering the compression chamber.

The aim of this investigation is to experimentally assess the quantity of liquid refrigerant (R-134a) exiting the muffler when injected at different velocities determined by the injection pressure. The muffler used in this experiment was part of a hermetic reciprocating compressor with a simplified transparent structure. Measurements were carried out for both the volume of liquid refrigerant collected after passing through the muffler and the injected mass. To facilitate observation of the flow inside the muffler, a high-speed camera recorded the injections through a transparent hatch.

2. METODOLOGY

2.1 Testbench layout

The bench was designed based on the principles of a calorimeter, utilizing a compressor that operates in a hot cycle. This section of the bench imposes specific boundary conditions on the muffler, including the mass flow rate, temperature and pressure of the refrigerant. A schematic of the bench shown in Figure 1 includes various components: a compressor (C), two electrical heaters (EH), two liquid separators (LS), a refrigerant buffer (RB), suction and discharge control valves (SV and DV), temperature sensors (T), pressure sensors (P), solenoid valves (S) and the test section (TS), where the muffler is placed. The temperature sensors are T-type thermocouples with an uncertainty of ± 0.5ºC, and the pressure sensors have uncertainties of ± 0.025 bar for suction and ± 0.06 bar for discharge. The test section, where the muffler is connected in series with the compressor to drive the gas flow, includes a pressure sensor with an uncertainty of ± 0.025 bar.

Figure 2 presents a p-h diagram that marks the corresponding points of the bench (1, 2, a, b, c, d). The desired operating condition is achieved by controlling the valves (SV and DV) and thermal heaters (EH), ensuring the cycle remains in the superheated vapor region. The liquid separator following the test section prevents refrigerant from directly entering the compressor, while the downstream separator collects and returns the compressor oil. The refrigerant buffer (RB) acts as a reservoir to manage any excess bench charge, essential for achieving the desired operating condition. The solenoid valves (S1 and S2) are used to interrupt the flow in the test section, a necessary step for measuring the volume of collected liquid refrigerant. Solenoid valve S4 allows the supply of refrigerant to the liquid refrigerant section (LRS), where the liquid refrigerant is formed to conduct the test by opening valve S3.

Figure 3 shoes the schematic of the liquid refrigerant section bench, which incorporates a closed-loop concept that connects to the hot gas section (HGS) through two solenoid valves (S3 and S4). This section of the bench is responsible for condensing the refrigerant fluid and ensuring it reaches the required pressure for testing. accordingly, the refrigerant supplied by valve S4 has its pressure increased by the compressor (C) and it is subsequently condensed by a heat exchanger with forced ventilation. Once condensed, this liquid is stored in a reservoir (LR) when valve S6 is opened. A check valve ensures that the liquid remains in the reservoir. Once the liquid formation process is complete, valve S6 is closed and valve S5 is opened, allowing the refrigerant to circulate while the compressor continues to operate. The auxiliary suction control valve (SAV) and the condenser fan shutdown prevent liquid from returning to the compressor. To reach the desired pressure, a pump circulates a mixture of water and propylene glycol within the

liquid reservoir (LR), regulated by temperature control. The pressure in the reservoir is monitored by a pressure sensor (± 0.04 bar uncertainty). Additionally, a probe-type thermocouple (± 1ºC uncertainty) measures the temperature of the liquid refrigerant. A load cell is also employed to monitor the weight of the refrigerant in the reservoir.

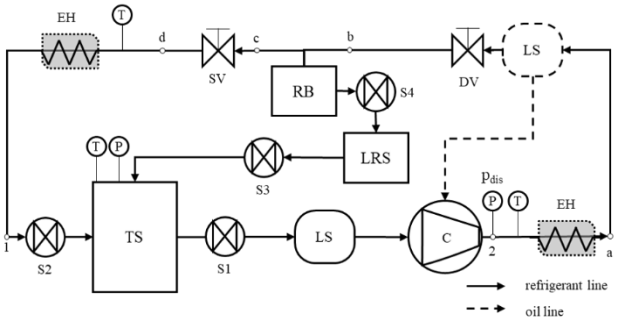

Figure 1: Testbench hot-cycle schematic

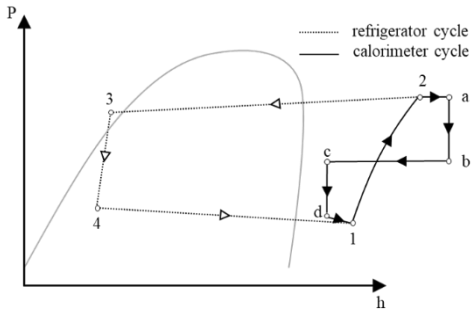

Figure 2: p-h diagram of calorimeter and refrigerator cycle

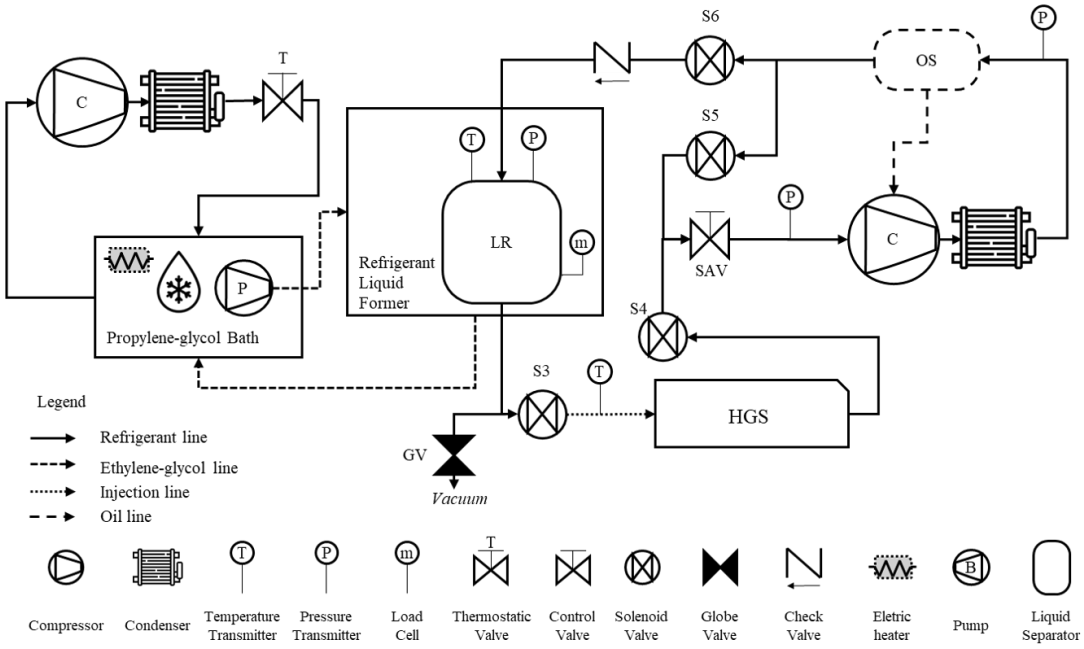

Figure 3: Testbench schematic

2.2 Muffler and test section

The muffler simplification, based on the methodology described by Rodrigues (2018), is illustrated in Figure 4. The collector block and muffler assembly are attached to a coordinate system. The injector tube is positioned horizontally and concentrically with the muffler inlet tube, separated by 20 mm, as depicted in Figure 5. To visualize the flow of liquid refrigerant inside the muffler, a high-speed camera (Phantom v12.1) is strategically at the front. This camera captures images at a resolution of 896x560 pixels and a frame rate of 1500 fps. Figure 6 shows three liquid collectors arranged in series, each equipped with graduation marks to facilitate the measurement of collected refrigerant volume. Additionally, a second camera (720p/24fps) records the collector, allowing for the subsequent measurement of the volume exiting the muffler.

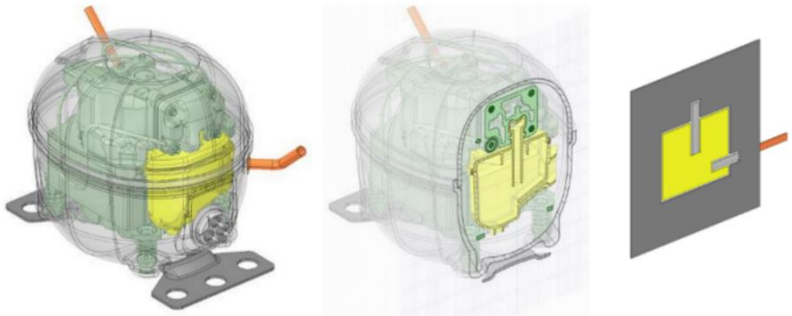

Figure 4: Muffler**. Source**: **(Rodrigues, 2018)**

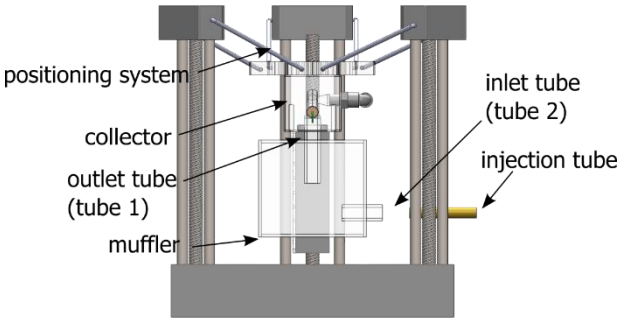

Figure 5: Test section front view

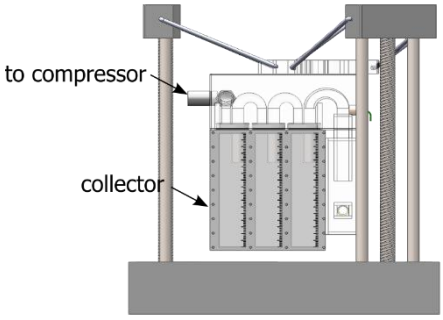

Figure 6: Test section isometric view

2.3 Test procedure

A reference system, under hot gas defrost, was used to take the operating conditions, the injection pressures and liquid mass injected. The tests were conducted using the following procedure: **(i)** Initially, the refrigerant is condensed in the liquid reservoir (LR). To achieve this, the liquid section compressor is activated, valves S4 and S6 are opened, and valve S5 is closed. The condenser fan remains operational throughout this process. This step continues until the mass of refrigerant reaches twice the required amount for the tests. Subsequently, valves S4 and S6 are closed, and valve S5 is opened. **(ii)** The propylene glycol bath system, which includes the compressor and electrical resistance, is then activated along with the pump. The pump circulates fluid around the liquid reservoir (LR) to attain the desired injection pressure. **(iii)** The test bench is set to the operating conditions: evaporating temperature T_e = -23.3ºC (p_e = 1.15 bar), condensing temperature T_c = 10.4ºC (p_c = 4.21 bar), test section temperature T_{ts} = 25ºC, and compressor speed = 3000 RPM, resulting in a mass flow rate of 11.92 kg/h. These conditions were set to match up with the evaporating temperature and the mass flow of the reference system. **(iv)** Once the conditions mentioned in (iii) and the desired injection pressure are achieved, the bath pump is stopped to prevent interference from the propylene glycol flow while measuring the refrigerant mass in the reservoir (LR). **(v)** The solenoid valve (S3) is then opened, initiating the injection process. This valve remains open until the desired mass of refrigerant is injected. At this point, the high-speed camera is triggered. **(vi)** After closing valve S3, the compressor is turned off, and valves S1 and S2 are closed to halt the gas flow. This allows the refrigerant liquid to be accommodated in the accumulator. **(vii)** Throughout the injection process, a second camera positioned in front of the collector (Figure 6) records the test. **(viii)** The footage captured in (vii) is subsequently processed to calculate the volume of liquid refrigerant collected from the muffler.

3. RESULTS

Björk & Palm (2006) conducted an experimental investigation and found that the refrigerant charge in the evaporator of a steady-state refrigeration system ranges from 30% to 45% of the total system charge. The reference system has a nominal load of 250 g. In a worst-case scenario where all the mass in the evaporator reaches the compressor, between 75 g and 112 g of refrigerant would need to be injected. Initial tests indicated that charges around 150 g led to saturation in the muffler and collector, preventing the measurement of the total liquid volume exiting the muffler. Regarding injection pressure, a value between the compressor discharge and suction pressures of the reference system was selected, since that is a possible range in a hot gas defrost. Consequently, tests were conducted with three different injection pressures (2, 4, and 6 bar) and three injected masses (25, 75, and 100g) for each pressure, totaling nine tests.

Each test was repeated seven times. The volume collected and injection mass flow rates were assessed to ensure they followed a normal distribution. Table 2 presents the average values and expanded uncertainties (95%) of the operating conditions for the nine tests. These conditions include discharge pressure (p_{dis}), suction pressure (p_{suc}), test section pressure (p_{ts}), and the temperatures of the suction line (T_{sl}), test section (T_{ts}), and injector tube (T_{inj}). The maximum uncertainties for the operational condition variables are as follows: 0.17 bar for discharge pressure, 0.06 bar for suction and test section pressures, 1.22°C for suction line temperature, 1.75°C for test section temperature, and 1.36°C for injector tube temperature.

Table 1: Operating conditions (pressure and temperature): means and expanded uncertainty (95%).

Test	Pressure [bar]	Mass [g]	p_{dis} [bar]		p_{suc} [bar]		p_{ts} [bar]		T_{sl} [ºC]		T_{ts} [ºC]		T_{inj} [ºC]	
			ref: 4.21		ref: 1.15		ref: 1.38		ref: 32		ref: 29		ref: 25	
			mean	U	mean	U	mean	U	mean	U	mean	U	mean	U
1		**50**	10.92	± 0.16	1.37	± 0.06	1.37	± 0.06	32.15	± 1.20	30.26	± 1.63	25.10	± 1.23
2	**2**	**75**	10.99	± 0.16	1.38	± 0.06	1.38	± 0.06	31.97	± 1.19	29.44	± 1.60	25.29	± 1.36
3		**100**	10.98	± 0.16	1.38	± 0.06	1.38	± 0.06	31.96	± 1.22	28.87	± 1.70	25.32	± 1.27
4		**50**	10.95	± 0.15	1.37	± 0.06	1.37	± 0.06	32.04	± 1.19	29.61	± 1.63	24.69	± 1.33
5	**4**	**75**	11.00	± 0.16	1.38	± 0.06	1.38	± 0.06	32.04	± 1.19	28.91	± 1.62	24.82	± 1.26
6		**100**	10.92	± 0.16	1.37	± 0.06	1.37	± 0.06	31.99	± 1.21	28.82	± 1.50	24.96	± 1.31
7		**50**	10.91	± 0.15	1.37	± 0.06	1.37	± 0.06	31.96	± 1.19	29.02	± 1.58	25.08	± 1.30
8	**6**	**75**	10.92	± 0.17	1.37	± 0.06	1.37	± 0.06	32.04	± 1.18	28.94	± 1.75	24.89	± 1.28
9		**100**	10.92	± 0.16	1.37	± 0.06	1.37	± 0.06	31.86	± 1.20	28.79	± 1.61	25.50	± 1.23

3.1 Liquid refrigerant collected

Table 2 presents the means and expanded uncertainties (95%) of the injection variables, namely injection pressure (Δp_{inj}), injected mass (m_{injd}), injection mass flow rate ($\dot{m}_{inj}$), injected volume estimation (V_{injd}), and volume collected after the muffler (V_{col}). The injection pressures exhibited minimal variation, while the injected mass showed greater variability, yet stayed close to reference values. The injection mass flow rate increased with higher injection mass and pressure. The estimated injected volume was primarily influenced by the amount of refrigerant injected and showed limited variation with pressure. The final column of the table represents the measured volume of liquid refrigerant exiting the muffler. As observed in the numerical simulations by Rodrigues (2018), there is a direct relationship between the injected mass and the collected volume, indicating that an increase in injected mass results in a higher volume of refrigerant fluid collected.

Table 2: Results: means and expanded uncertainty (95%).

Test	Pressure [bar]	Mass [g]	Δp_{inj} [bar]		m_{injd} [g]		$\dot{m}_{inj}$ [kg/h]		V_{injd} [ml]		V_{col} [ml]	
			ref: 2/4/6		ref: 50/75/100		-		-		-	
			mean	U	mean	U	mean	U	mean	U	Mean	U
1		**50**	2.01	± 0.12	51.77	± 1.85	33.00	± 1.28	40.97	± 1.78	1.33	± 0.21
2	**2**	**75**	2.00	± 0.11	76.84	± 1.68	38.82	± 1.29	60.77	± 1.56	3.92	± 0.60
3		**100**	2.00	± 0.11	101.64	± 1.67	42.22	± 1.26	80.33	± 1.56	10.82	± 1.32
4		**50**	4.00	± 0.11	52.94	± 2.08	40.97	± 1.91	43.51	± 2.11	2.67	± 0.26
5	**4**	**75**	4.01	± 0.11	77.38	± 1.81	49.99	± 1.36	63.55	± 1.78	3.94	± 0.26
6		**100**	4.00	± 0.11	102.79	± 2.27	55.36	± 1.47	84.32	± 2.32	5.49	± 0.44
7		**50**	6.00	± 0.12	53.83	± 2.11	44.95	± 1.93	45.72	± 2.20	3.93	± 0.20
8	**6**	**75**	5.99	± 0.12	78.38	± 2.07	54.64	± 1.64	66.49	± 2.19	5.64	± 0.62
9		**100**	5.99	± 0.12	102.01	± 2.01	60.81	± 1.59	86.46	± 2.10	7.19	± 0.60

Figure 7 shows the relationship between the average collected volume and injection pressures across three injected masses, with uncertainty bars representing the 95% confidence interval. Generally, there is a direct correlation between the collected volume and injection pressure, except for the injected masses of 100 g and 75 g. Notably, when the injection pressure increases from 2 to 4 bar for a 100 g injected mass, the collected volume decreases. However, no significant change is observed in the 75 g injection at the same pressure variation. This divergence in trends between 100 g and 75 g tests is likely due to changes in the flow dynamics of liquid refrigerant within the muffler. In Figure 8, tests at 2 bar injection pressure exhibit distinct behavior compared to others. The standard deviations follow the same trends of the collected volume and are an order of magnitude smaller than the average values.

The ratio the collected volume to the injected volume of fluid is an important indicator of the refrigerant's tendency to exit the muffler under specific test conditions. Figure 9 presents this ratio in a bar graph, where the empty bars represent the average injected volume, and the hatched bars represent the average collected volume. The corresponding percentage ratio between the two volumes is also shown. It is worth noting that, at an injection pressure of 2 bar, this ratio significantly increases as the injected mass increases. Figure 10 offers an alternative representation of these results, plotting the percentage ratio between volumes against the injected mass. These figures show that, except at an injection pressure of 2 bar, the ratio between the collected and injected volumes remains relatively constant regardless of the injected mass, and is primarily influenced by the pressure.

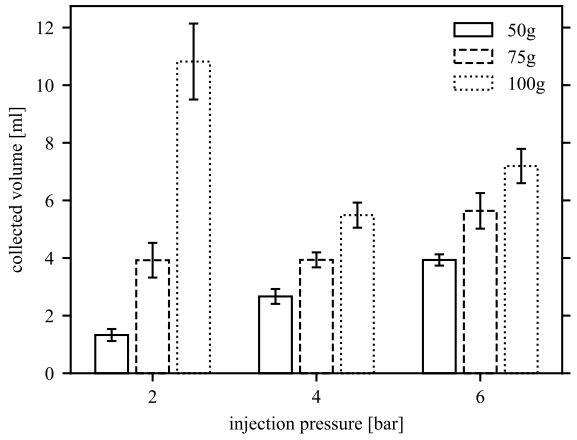

Figure 7: Collected volume mean and uncertainty by injection pressure.

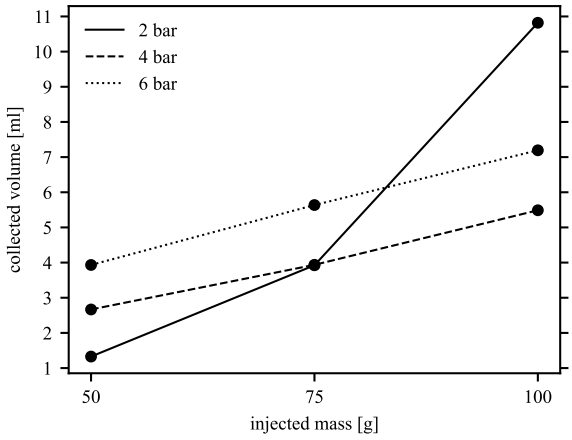

Figure 8: Collected volume mean and uncertainty by injected mass

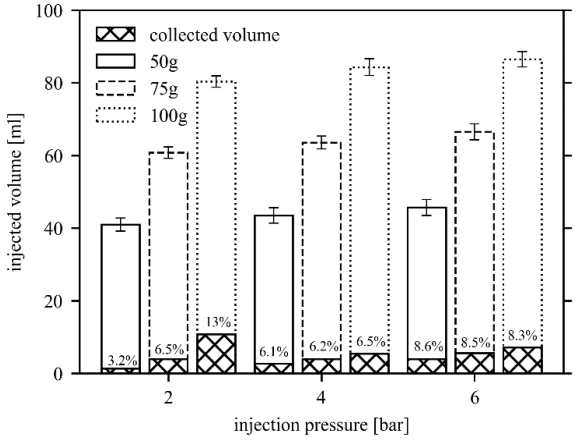

Figure 9 Injected volume mean and uncertainty, collected volume mean.

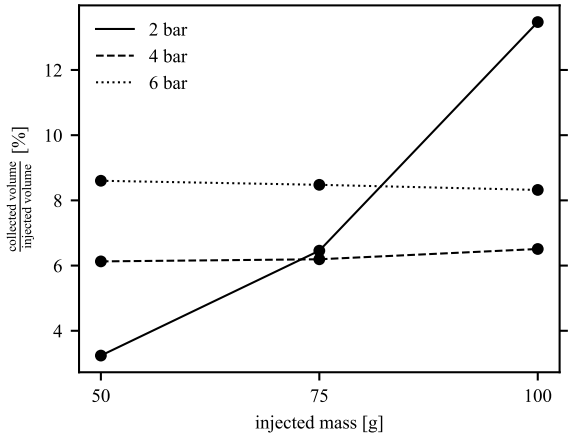

Figure 10: Collected by injected volume means

3.3 The liquid suction mechanism

Two distinct liquid refrigerant suction mechanisms were observed in the study. The first mechanism, referred to as type 1, is depicted in Figure 11. In this mechanism, the liquid refrigerant can either flow directly from the inlet to the outlet tube or collide with the opposite wall of the muffler before reaching the outlet tube. On the other hand, the second mechanism, named as type 2, is illustrated in Figure 12. In this mechanism, the liquid moves upwards along the opposite wall and the upper wall until it reaches the side and entrance of the outlet tube, where it is suctioned. During the initial moments of the injection, when the muffler is empty, the type 1 mechanism is more relevant. However, as the muffler becomes filled with liquid refrigerant, the type 2 mechanism becomes more pronounced. This intensification of the type 2 mechanism primarily occurs when the volume of liquid inside the muffler reaches the height of the inlet, as shown in Figure 13. Conversely, when the volume of liquid exceeds the height of the inlet tube, as depicted in Figure 14, a jet of liquid refrigerant from the inlet collides with the liquid layer covering the opposite wall, reducing its momentum and forming a vortex inside the muffler. This hinders the liquid's motion to the opposite upper quadrant and increases its flow towards the outlet tube, reducing the prevalence of the type 2 mechanism and favoring type 1. After the injection ends and the solenoid valve in the injector tube closes, it is observed that liquid refrigerant keeps filling the muffler as long as the compressor remains on. At this stage, the gas flow drags liquid directly to the muffler outlet, which corresponds to the type 1 mechanism.

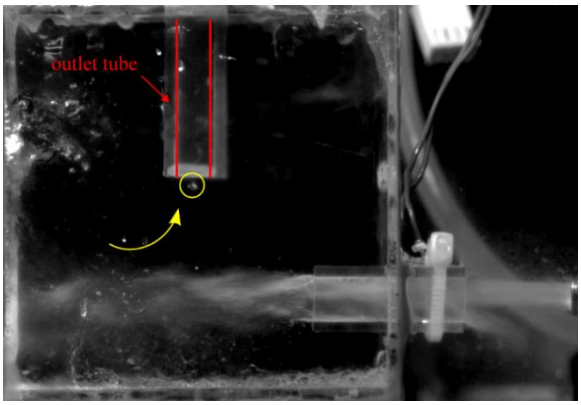

Figure 11: Suction mechanism (type 1).

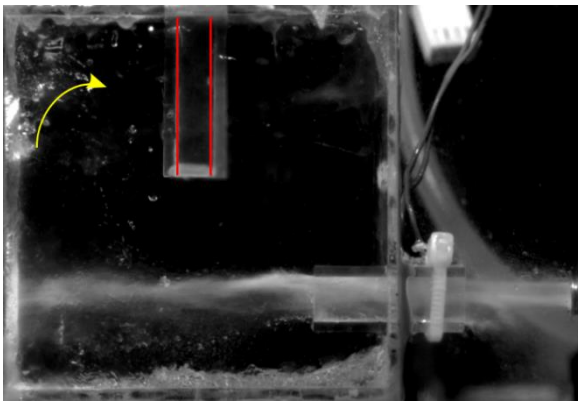

Figure 12: Suction mechanism (type2).

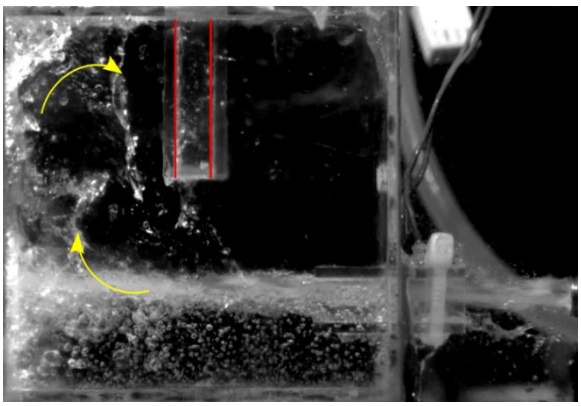

Figure 13: Suction mechanism (type 2) with muffler full.

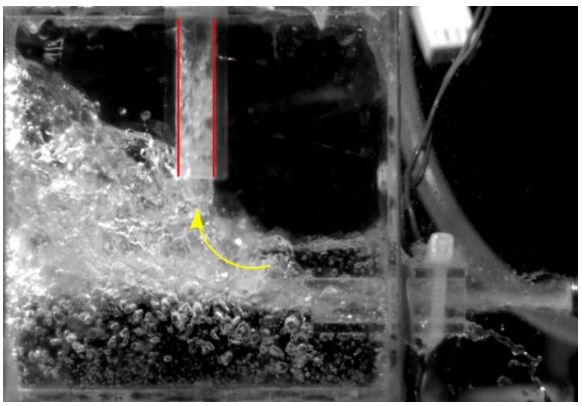

Figure 14: Suction mechanism (type 1) with muffler full.

Higher injection pressure leads to a jet from the inlet with greater momentum and a broader spread of liquid refrigerant within the muffler. This spreading effect enhances the type 2 suction mechanism as the outlet tube becomes saturated. It is worth noting that this phenomenon occurs sooner when the jet collapses early at higher pressure levels. Additionally, a larger quantity of injected mass also enhances the spreading effect. This flow dynamics is evident when comparing the results of tests conducted at 2 bar (Figure 15) and 6 bar (Figure 16), both with an injection mass of 50 g and the same fraction of elapsed test time (40%).

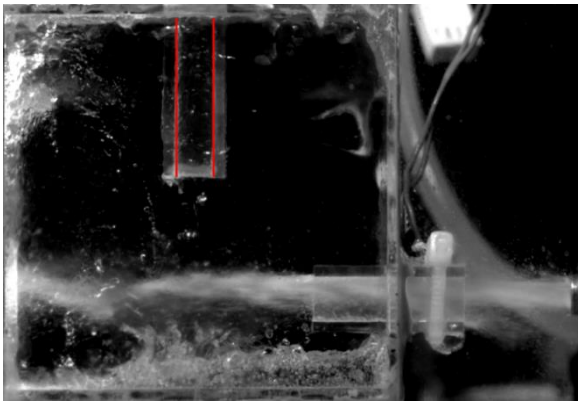

Figure 15: Pressure liquid spreading influence. Test 1 (2 bar, 50g).

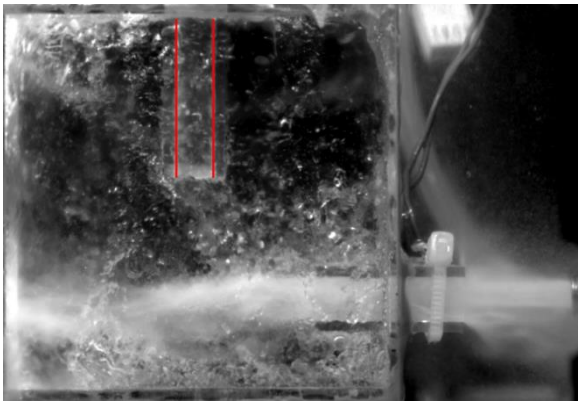

Figure 16: Pressure liquid spreading influence. Test 7 (6 bar, 50g).

In the initial tests conducted with an injection pressure of 2 bar (tests 1, 2 and 3), it was observed that the low jet momentum was insufficient to generate a significant suction and liquid spreading. However, as the muffler gradually filled up, aided by the relatively low momentum, the liquid eventually reached the inlet tube level. At this point, the jet drags liquid from the bottom surface, leading to the dominance of the type 2 suction mechanism, as depicted in Figure 13. At this moment, the 50 g test (test 1) it ceased, but for 75 and 100 g the process continued, causing the liquid level to surpass the inlet tube level. Consequently, the difference in liquid level prompted a transition to the type 1 mechanism, as illustrated in Figure 14.

As the injection pressure increases, the spreading process occurs faster and more intensely, which in turn promotes suction through the type 2 mechanism. When the liquid level reaches the inlet tube, the increased injection pressure intensifies the impact of the jet on the liquid surface, thereby reinforcing the type 2 mechanism as depicted in Figure 13. However, at injection pressures of 4 bar and 6 bar, the liquid volume entering the muffler is insufficient to surpass the level of the inlet tube and transition the suction regime from type 2 to type 1, unlike the condition observed at 2 bar shown in Figure 14. The main challenge for the jet to entering the muffler at higher injection pressures, despite its greater momentum, is the early jet collapse due to the increased inertia force at the boundary between the jet and the surrounding environment. This reduced stability leads to an early collapse of the jet. In tests conducted with injection pressures of 4 and 6 bar, the injected mass extends the injection process and results in a higher liquid level, explaining the greater volume collected at these pressures with an increase in injected mass. The rise in pressure also leads the jet to spread wider, causing the outlet tube to become saturated and favoring the type 2 suction mechanism. After closing the injection valve, the compressor continues to operate for an additional second, with the gas flow trapping the liquid inside the muffler and maintaining the liquid refrigerant suction. The final liquid level retained in the muffler depends on the injected mass but is inversely proportional to the injection pressure.

To summarize, the dispersion of the liquid is influenced by the increase in pressure, resulting in a larger volume collected in the 6 bar injection tests compared to the 4 bar tests, despite having the same mass. Additionally, increasing the mass injected in the 4 and 6 bar tests leads to a greater volume of liquid collected, as the increase in mass prolongs the injection process and a higher liquid level is achieved. Moreover, when the inlet tube is flooded in refrigerant fluid during the 2 bar tests with masses of 75 and 100 g, a change in the suction mechanism occurs, as depicted in Figure 14. This change, combined with the suction caused by the gas flow, significantly contributes to the liquid refrigerant exiting the muffler. This flow dynamics is consistent with the findings in Figure 8, where the curves of collected volume as a function of injected mass, separated by injection pressure, exhibit similar behavior for the 4 bar and 6 bar tests, with higher values for higher pressures. Furthermore, an increase in collected volume is observed with increased injected mass at the same pressure. The distinct behavior of the curve for 2 bar appears to be consistent with the demonstrated transition, where both variables experience a jump for 75 g and 100 g.

4. CONCLUSIONS

The experimental results for liquid refrigerant injection in the suction muffler of a small reciprocating compressor revealed a clear correlation between the volume collected, mass injected, and injection pressure. An increase in both injection pressure and injected mass led to higher mass injection flows, although the rate of increase diminished as these variables increased. The ratio of collected to injected volumes remained constant at higher injection pressures, regardless of the mass injected. In contrast, at lower injection pressures, a distinct pattern was observed when larger refrigerant masses were injected. In these conditions, a significant increase in collected volume indicated a direct correlation between the ratio of collected to injected volumes with the injected mass. Further analysis showed that higher injection pressures led to a quicker and more intense dispersion of the liquid within the muffler, increasing the collected volume. Additionally, higher injection pressures caused the jet from the inlet to collapse earlier, reducing the volume of liquid that enters the muffler. At low injection pressures, the muffler became fuller and a transition occurred in the liquid suction dynamics. This transition was characterized by gas flow favoring the removal of refrigerant from the muffler, which explains the greater volume collected with lower injection pressures.

NOMENCLATURE

m	mass	[g]	**Subscript**	
$\dot{m}$	mass flow	[kg/h]	c	condensing
p	pressure	[bar]	col	collected
T	temperature	[ºC]	dis	discharge
U	expanded uncertainty	[x]	e	evaporating
V	volume	[ml]	inj	injection
			injd	injected
			sl	suction line
			suc	suction
			ts	test section

REFERENCES

Balconi, T. B., Rodrigues, T. T., & Deschamps, C. J. (2022). Experimental Investigation of Liquid Slugging in the Suction Mufflers of Hermetic Reciprocating Compressors. *Proceedings of the 26th International Compressor Engineering Conference, (Paper 2744)*. https://docs.lib.purdue.edu/icec/2744/

Bianchi, M., Deschamps, C. J., Rodrigues, T. T., & Paladino, E. E. (2021). Numerical-experimental investigation of liquid slugging in the suction muffler of a hermetic reciprocating compressor. *Materials Science and Engineering Conference Series*, *1180*, 12017. https://doi.org/10.1088/1757-899X/1180/1/012017

Björk, E., & Palm, B. (2006). Refrigerant mass charge distribution in a domestic refrigerator. Part II: Steady state conditions. *Applied Thermal Engineering*, *26*(8–9), 866–871. https://doi.org/10.1016/j.applthermaleng.2005.10.004

Brendel, L. P. M., Pranatharthi Haran, S., Liu, H., Braun, J. E., & Groll, E. A. (2023). Correlation to predict conditions that lead to liquid-flooding at compressor start-up as a function of evaporator size and fluid properties. *International Journal of Refrigeration*, *146*, 349–356. https://doi.org/10.1016/j.ijrefrig.2022.11.017

Embraco - Nidec. (2022). *Hot Gas Defrost*. https://www.embraco.com/wp-content/uploads/2022/06/technical-information-hot-gas-defrost.pdf

Laughman, C. R., Norford, L. K., & Leeb, S. B. (2006). The Detection of Liquid Slugging Phenomena in Reciprocating Compressors via Power Measurements. *International Compressor Engineering Conference*, *1986*, 1–8.

Liu, Z., & Soedel, W. (1995). A Mathematical Model for Simulating Liquid and Vapor Two-Phase Compression Processes and Investigating Slugging Problems in Compressors. *HVAC\&R Research*, *1*(2), 99–109. https://doi.org/10.1080/10789669.1995.10391312

Rodrigues, T. T. (2018). Refrigerant Liquid Slugging In The Suction System of Reciprocating Compressor. *Proceedings of the 24th International Compressor Engineering Conference, (Paper 2523)*. https://docs.lib.purdue.edu/icec/2523/

Secop. (2019). *Hot Gas Defrost with Secop Compressors*. https://www.secop.com/fileadmin/user_upload/technical-literature/product-bulletins/compressors/hotgas_defrost_with_secop_compressors_01-2019_desn600d102.pdf

Singh, R., Nieter, J. J., & Prater, G. (1986). Investigation of the compressor slugging phenomenon. *ASHRAE Transactions*, *92*(pt 1B), 250–258.

Stouppe, D. E., & Lau, T. Y. S. (1989). Air conditioning and refrigeration equipment failures. *National Engineer*, *93*(1989), 14–17.

ACKNOWLEDGEMENT

The present study was developed as part of a technical-scientific cooperation program between the Federal University of Santa Catarina and NIDEC-GA. Additional funding was provided by the National Institutes of Science and Technology (INCT) Program (CNPq Grants 404023/2019-3 and 131645/2019-6; FAPESC Grant 2019TR0846) and EMBRAPII Unit POLO/UFSC. Technical support from Eduardo L. Silva is duly acknowledged.